Accepted Manuscript

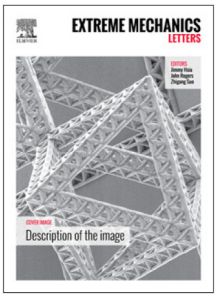

Deflected trajectory of a single fluid-driven crack under anisotropic *in-situ* stress

Fuqiang Sun, Wenhao Shen, Ya-Pu Zhao

PII: S2352-4316(19)30045-8
DOI: https://doi.org/10.1016/j.eml.2019.100483
Article number: 100483
Reference: EML 100483

To appear in: *Extreme Mechanics Letters*

Received date : 26 March 2019
Revised date : 16 May 2019
Accepted date : 19 May 2019

Please cite this article as: F. Sun, W. Shen and Y.-P. Zhao, Deflected trajectory of a single fluid-driven crack under anisotropic *in-situ* stress, *Extreme Mechanics Letters* (2019), https://doi.org/10.1016/j.eml.2019.100483

Deflected trajectory of a single fluid-driven crack under anisotropic *in-situ* stress

Fuqiang Sun[a,b], Wenhao Shen[a,c] and Ya-Pu Zhao[a,b,*]

[a] *State Key Laboratory of Nonlinear Mechanics, Institute of Mechanics, Chinese Academy of Sciences, Beijing 100190, China*

[b] *School of Engineering Science, University of Chinese Academy of Sciences, Beijing 100049, China*

[c] *Institute of Applied Mechanics, Taiyuan University of Technology, Taiyuan 030024, China*

ABSTRACT

Deflected crack trajectories are detected in hydraulic fracturing. There are numerous physical quantities impacting the deflection of a fluid-driven crack. A 2D model of the elasto-hydrodynamics system is established to predict the crack trajectory and to investigate the coupling effects of anisotropic *in-situ* stress, fluid viscosity, fluid injection rate and crack inclination on the crack deflection. The displacement discontinuity method (DDM) and the finite difference method (FDM) are used to solve the nonlinear problem. The concept of deflection region is defined to quantify the crack deflection. Results show that the size of the deflection region is dominated by the inclination angle. Increase of the magnitude and the difference of *in-situ* stresses promotes crack deflection. The combined effects of fluid viscosity and fluid injection rate are divided into three stages: significant prevention stage, significant promotion stage and insignificant prevention stage. This study provides the method for crack trajectory prediction and crack deflection control.

Keywords: Hydraulic fracturing; *In-situ* stress; Deflection region; Crack trajectory.

* Corresponding author: yzhao@imech.ac.cn

1. Introduction

Hydraulic fracturing has been used to enhance the production of conventional and unconventional energy resources from underground reservoirs for decades. In the process, hydraulic fracturing trajectory is affected by the properties of reservoir rock, fracturing fluid, the magnitude and the direction of *in-situ* stress [1]. *In-situ* stress corresponds to the natural stress in the rock mass prior to any artificial disturbance. Mathematical models [2-14] and experiments [15-20] are developed to clarify the effects of the physical quantities and to explain the physical mechanism of hydraulic fracturing.

There are studies analyzing the propagation of the fluid-driven cracks. The studies revealed that a straight fluid-driven crack is in the toughness-dominate regime or in the viscosity-dominate regime, depending on the competition between fracture toughness and fluid viscosity in the propagation of the crack [3-5]. For a steadily propagating crack, which is driven by the Newtonian fluid, the size of the fluid-lag zone is revealed to stay constant, while it will decrease when *in-situ* stress increases [6-8]. Shen and Zhao [8-10] discussed the growth of a fluid-driven crack in a homogenous medium, and showed the potential shear-stress induced deflections of fluid-driven cracks. Since the fracturing operation is conducted at a great depth, where the minimum principal *in-situ* stress is typically in horizontal direction, multistage hydraulic fracturing in horizontal wellbores is reported [11-13] to economically develop unconventional resources in shale reservoirs. The fluid-driven cracks deflect if the incline angle of the wellbore is nonzero [1]. In a hydraulic crack system where multiple cracks propagate parallelly, the stress-shadow effect, referred as the strong interaction among closely spaced cracks, may cause suppression and deflection of fluid-driven cracks [13,14]. However, these investigations are under the assumption that the initial crack is perpendicular to the minimum principal *in-situ* stress and the fluid-driven crack propagates straightly along the direction of the maximum principal *in-situ* stress. If the initial crack is inclined to the principal *in-situ* stresses, what will the crack trajectories

be?

Field experiments [15,16] indicated that deflections and offsets of fluid-driven crack trajectories widely exist in hydraulic fracturing. Laboratory experiments [17,18] were conducted to investigate the trajectories of inclined fluid-driven cracks under uniaxial compressive stress. According to different trajectories, the deflected cracks are divided into different types: tensile crack, shear crack and mixed tensile-shear crack [17]. Whatever type it takes, the trajectories are finally along the direction of the maximum principal stress. Other triaxial-loading experiment investigations [19,20] also indicated that the magnitude and direction of *in-situ* stress should be considered in the prediction of fluid-driven crack trajectory. However, the effects of the physical quantities, including *in-situ* stress, fluid viscosity, fluid injection rate and crack inclination angle, still need to be clarified for the prediction of the deflected trajectories.

As shown in Fig. 1, a fluid-driven crack trajectory in an infinite elastic rock medium is studied. The highly pressurized fracturing fluid, which is forced into the crack, introduces stresses on the crack surfaces, resulting in the opening and the propagation of crack in the elastic medium. During the study of hydraulic fracturing, the rock is assumed to be homogeneous, isotropic and impermeable. The stresses σ_1^∞ and σ_2^∞ correspond to the anisotropic *in-situ* stress, with σ_1^∞ and σ_2^∞ being the maximum and the minimum principal *in-situ* stress, respectively [21]. The principal *in-situ* stresses remain constant with the crack propagation. Assume that there is no lag zone at the crack tip. The injected viscous fluid is modeled as the Newtonian and incompressible fluid, and the system is assumed in the toughness-dominant regime.

This paper is organized as follows. Firstly, a 2D model of hydraulic fracturing is established and validated, using the theories of lubrication flow and linear elastic fracture mechanics (LEFM). Secondly, crack trajectories are predicted, and the stress field near the crack surfaces is studied. Thirdly, the effects of physical quantities, such as inclination angle, injection rate, fluid viscosity and *in-situ* stress, on the deflected

trajectories of fluid-driven cracks, are clarified. At last, the mechanism of the fluid-driven crack deflection is discussed.

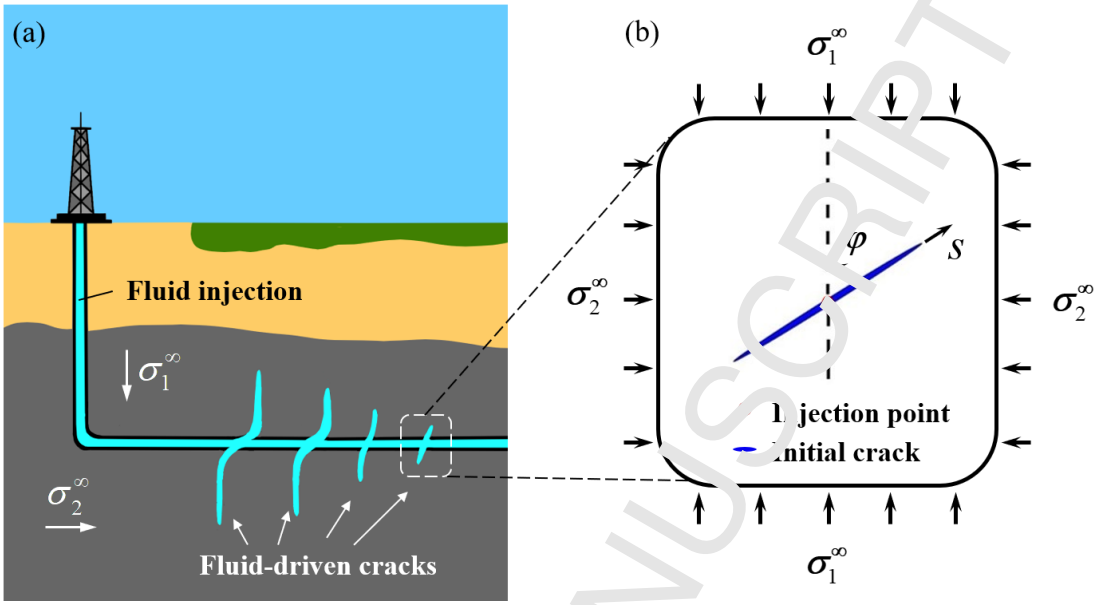

Fig. 1. (a) Schematic of the crack deflection in fracturing operation. (b) Model of the initial crack. φ is the inclination angle, σ_1^∞ and σ_2^∞ are the maximum principal *in-situ* stress and the minimum principal *in-situ* stress, respectively. The initial crack is inclined to the principal *in-situ* stresses.

2. Model Development

The geometry and boundary conditions are symmetric about the inlet of fracturing fluid, as shown in Fig. 1(b). Hence a curvilinear coordinate system is used, with the origin O being at the inlet of the fracturing fluid, coordinate axis s being along with the crack trajectory, coordinate n being perpendicular to the crack trajectory and φ being inclination angle, i.e., the angle between the crack trajectory and the direction of the maximum principal stress. According to the symmetry of physical quantities, the governing equations and boundary-condition equations are described in the right half plane, where $s>0$.

2.1. Governing equations

The viscous flow of fracturing fluid is described by the lubrication theories without

body forces, for example, the nonlinear Reynolds equation [22]:

$$\frac{\partial w}{\partial t}=\frac{1}{12\eta}\nabla\cdot\left(w^3\nabla p\right), \tag{1}$$

which can be obtained by combining the continuity equation and the Poiseuille's law for a viscous flow:

$$\frac{\partial w}{\partial t}+\nabla\cdot\boldsymbol{q}=0, \tag{2}$$

$$\boldsymbol{q}=-\frac{w^3}{12\eta}\nabla p, \tag{3}$$

where η is the dynamic viscosity of fracturing fluid, w is the crack opening, p is the fluid pressure, and $\boldsymbol{q}$ is the fluid flux. These field quantities are functions of both the coordinate s and the time t.

The fluid pressure p is related to the boundary condition of stress in elasticity theory. According to Crouch [23], stress tensor $\boldsymbol{T}$ at any point within the elastic region is defined as the integral of displacement discontinuity $\boldsymbol{D}$ over the crack trajectory S:

$$\boldsymbol{T}(\xi)=\int_S \boldsymbol{\Xi}(\xi,\zeta)\cdot\boldsymbol{D}(\zeta)\,\mathrm{d}S(\zeta), \tag{4}$$

where the quantity $\boldsymbol{\Xi}$ is a rank-three tensor, representing the influences of the displacement discontinuity at ζ on the stress field at ξ in the elastic medium. Therefore, we can call it "displacement-stiffness tensor". This equation is further discussed in Appendix A.

LEFM is used to analyze the crack problem. As being widely used and validated in hydraulic fracturing simulations [8-10,12], the maximum circumferential stress criterion [24] is used in the simulation of crack propagation. In the criterion, a crack will propagate in the direction where the circumferential stress is maximal and reaches a critical value. When the critical stress is given by the fracture toughness K_{IC}, the maximum circumferential stress criterion can be expressed as:

$$\frac{1}{2}\cos\frac{\theta}{2}\left[K_{\mathrm{I}}\left(1+\cos\theta\right)-3K_{\mathrm{II}}\sin\theta\right]=K_{\mathrm{IC}}, \tag{5}$$

where K_{I} and K_{II} are the stress intensity factors (SIFs) of mode I and mode II

fracture, respectively, and θ is the deflection angle of the crack trajectory, which satisfies:

$$K_{\mathrm{I}}\sin\theta+K_{\mathrm{II}}(3\cos\theta-1)=0. \tag{6}$$

The boundary conditions are expressed as follows:

$$\begin{aligned}&\sigma^s=\sigma_1^\infty\sin\theta+\sigma_2^\infty\cos\theta,\ \sigma^n=\sigma_1^\infty\cos\theta-\sigma_2^\infty\sin\theta-p,\\&q_{s=0}=q_0,\ q_t=0,\end{aligned} \tag{7}$$

where σ^s and σ^n are shear and normal stresses at crack surfaces, respectively, $q_{s=0}$ is the fluid flow rate at inlet, q_0 is the fluid injection rate, and q_t is the flow rate at the crack tip.

2.2. Numerical method

The model of the crack trajectory simulation is based on the displacement discontinuity method (DDM), which is a kind of boundary element method. The method is developed by Crouch [23] and designed for handling problems with crack-like geometries. In DDM, for a N-elements problem, the normal and the shear displacement discontinuities can be calculated by the equation:

$$\sigma_i^s=\sum_{j=1}^{N}\left(C_{ij}^{ss}D_j^s+C_{ij}^{sn}D_j^n\right),\ \sigma_i^n=\sum_{j=1}^{N}\left(C_{ij}^{ns}D_j^s+C_{ij}^{nn}D_j^n\right), \tag{8}$$

where C_{ij}^{ss}, C_{ij}^{sn}, C_{ij}^{ns} and C_{ij}^{nn} are boundary stress influence coefficients. The coefficient C_{ij}^{sn}, for example, gives the actual shear stress at element i (σ_i^s) due to a constant unit normal displacement discontinuity of element j (D_j^n). In this simulation, we use piece-wise constant displacement discontinuity elements with the middle points of each element being the collocation points.

Finite difference method (FDM) is used to solve the equations of the elasto-hydrodynamics system. In this model, the crack opening is obtained by Eq. (8). The SIFs are measured by the crack opening, under the assumption that the fluid-driven

crack is in the toughness-dominant regime, where the crack is elliptical [8]. We take the following equations derived by Olson [12]:

$$K_{\mathrm{I}} = \frac{E\sqrt{\pi}}{4\left(1-\nu^2\right)\sqrt{a}} w_t, \quad K_{\mathrm{II}} = \frac{E\sqrt{\pi}}{4\left(1-\nu^2\right)\sqrt{a}} v_t, \tag{9}$$

where E is the Young's modulus, ν is the Poisson's ratio, a is the length of the crack tip element, $w_t = cD_{\mathrm{tip}}^n$ and $v_t = cD_{\mathrm{tip}}^s$ are corrected normal and shear crack openings at the crack tip element, respectively. The correction factor $c = 0.806$, D_{tip}^n and D_{tip}^s are normal and shear displacement discontinuities of the tip element, respectively.

2.3. Normalization

For the convenience of further analysis, the normalized form of governing equations is taken. The normalization scheme is as follows:

$$s = l_0\tilde{s}, \quad a = l_0\tilde{a}, \quad w = \varepsilon l_0\tilde{w}, \quad p = \Lambda\tilde{p}, \quad q_i = q_0\tilde{q}_i \text{ and } t = M\tilde{t}, \tag{10}$$

in which l_0 is the initial crack radius. ε, Λ and M are time-independent quantities, which are obtained by substituting normalization scheme into Eqs. (2), (3), (5), (7), (8) and (9). The mass conservation must be ensured. Normal and shear displacement discontinuities of tip element is measured by crack opening. With the assumption that the system is in the toughness-dominant regime, the fracture toughness is used to measure the fluid viscosity. Consequently, Eqs. (2) and (8) are normalized, and the quantities are derived as:

$$\varepsilon = \frac{8\left(1-\nu^2\right)K_{\mathrm{IC}}}{E\sqrt{\pi l_0}}, \quad M = \frac{8\left(1-\nu^2\right)K_{\mathrm{IC}}l_0^{3/2}}{q_0E\sqrt{\pi}} \text{ and } \Lambda = \frac{4\left(1-\nu\right)K_{\mathrm{IC}}}{\sqrt{\pi l_0}}. \tag{11}$$

Then, other dimensionless quantities are obtained:

$$\tilde{\eta} = \frac{3\pi E^3 q_0\eta}{512\left(1+\nu\right)^3\left(1-\nu\right)^4 K_{\mathrm{IC}}^4}, \quad \tilde{\sigma}_1^{\infty} = \frac{\sigma_1^{\infty}\sqrt{\pi l_0}}{4\left(1-\nu\right)K_{\mathrm{IC}}} \text{ and } \tilde{\sigma}_2^{\infty} = \frac{\sigma_2^{\infty}\sqrt{\pi l_0}}{4\left(1-\nu\right)K_{\mathrm{IC}}}, \tag{12}$$

where $\tilde{\eta}$ is the dimensionless fluid viscosity, $\tilde{\sigma}_1^{\infty}$ and $\tilde{\sigma}_2^{\infty}$ are the dimensionless principal *in-situ* stresses. It is evident that the dimensionless number $\tilde{\eta}$ represents the combined effect of both the physical properties of reservoirs and the real working conditions (the fluid viscosity and the fluid injection rate). For a given reservoir, $\tilde{\eta}$ is proportional to the product of the injection rate q_0 and the fluid viscosity η.

2.4. Validation

To validate the numerical model used in this simulation, as shown in Fig. 2, a case of uniformly pressurized radial crack is studied. The numerical results with different grids are checked by the following analytical solution [10]:

$$\tilde{w} = \frac{w}{\varepsilon l_0} = \frac{8\left(1-\nu^2\right)}{\pi E \varepsilon} p\sqrt{1-\tilde{s}^2} \,. \tag{13}$$

In the validation test, we take $\nu = 0.2$, $E = 1.5\times10^5$ Pa, $p = 10$ Pa and $\varepsilon = 1\times10^{-4}$. Fig. 2(b) shows that the results calculated by this numerical model are consistent with the analytical results. According to Eq. (9), as shown in Fig. 2(c), crack tip opening is validated to ensure the correctness of the SIFs calculation. In addition, as shown in Fig. 3, during the simulation process, the crack trajectory converges well with the increase of the mesh density.

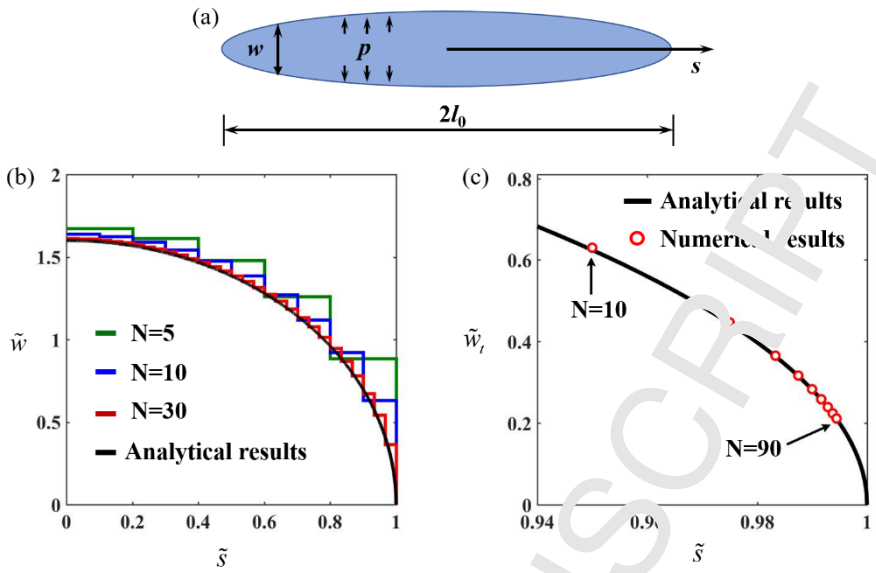

Fig. 2. (a) Schematic of the uniformly pressurized radial crack in the validation, where w is the crack opening, p is the fluid pressure, l_0 is the crack radius and s is the coordinate axis. (b) Crack opening comparison between numerical and analytical results, where N is the grid number. (c) Crack opening calculation of the tip element versus analytical results, where the grid number N ranges from 10 to 90 with an increment by 10.

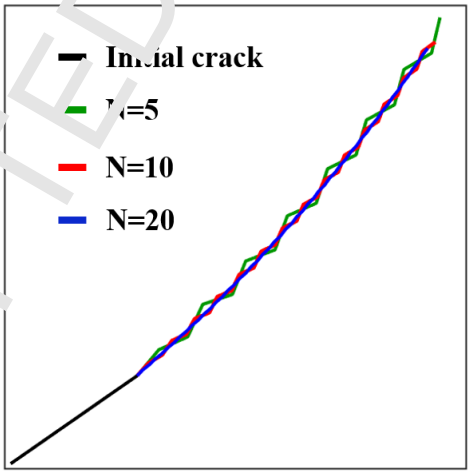

Fig. 3. Deflected crack trajectories predicted in different mesh densities, where N is the grid number of the initial crack.

3. Results and Discussions

In previous sections, the details of the hydraulic fracturing simulation model were

introduced and validated. In this section, we are going to investigate the stress field near the curved crack during the propagation process, and to quantitatively study the effects of the crack inclination angle, the viscosity of fracturing fluid and the anisotropic *in-situ* stress on the crack deflection, respectively.

3.1. Stress field

The stress field near the crack surface, especially the stress field near the crack tip, plays a dominant role in the crack propagation process [25]. How stresses are distributed and regularized near a crack's tip will dominate the mode of failure and may hold the key to resolving important open questions about issues such as crack stability and path selection [26,27]. In this subsection, the curved crack morphology at different time will be described during the crack propagation process. The stress field near the crack surfaces will also be investigated, corresponding to each crack morphology.

A preset crack with the inclination angle of 60 degrees is studied to describe the crack trajectory and investigate the stress field under the acting of the anisotropic *in-situ* stress. In this simulation, the dimensionless viscosity $\tilde{\eta} = 49$, the dimensionless stresses $\tilde{\sigma}_1^{\infty} = 0.174$, $\tilde{\sigma}_2^{\infty} = 1.57 \times 10^{-2}$.

As shown in Fig. 4, the crack trajectories at different time are pictured with the initial crack staying straight at $\tilde{t} = 0$. The crack trajectory deflects gradually towards the direction of the maximum principal stress under the effect of the *in-situ* stress. At $\tilde{t} = 40$, the inclination angle reaches 0 degree, which means that the crack propagates in the same direction as the maximum principal stress and the crack deflection process is completed. Here, the term 'deflection region' is defined as the region surrounded by the curved crack trajectory and the lines parallel to the direction of the maximum and the minimum principal stress, respectively. More details about the deflection region will be studied in the subsections 3.2-3.4.

The hydrostatic stress $\tilde{\sigma}_p = \left(\tilde{\sigma}_{11} + \tilde{\sigma}_{22}\right)/2$ and the shear stress $\tilde{\tau}_{12}$ in elastic

medium are described in Fig. 4(b) and Fig. 4(c), respectively. As shown in Fig. 4, with the injection of fracturing fluid, the crack inflates and the crack surfaces are expanded. Therefore, the hydrostatic stress in the vicinity of the crack surfaces stay compressive, while the hydrostatic stress near the crack tip remain tensile. Stress concentration occurs, and dominates the crack propagation. The contours also indicate that the stress field caused by fluid pressure is going to vanish at a distance roughly equaling to the crack length, within which will another crack be influenced by the stress field. The shear stress tends to be zero at the vicinity of the crack surfaces.

During the deflection process, the fluid-driven crack propagates symmetrically from initial crack tips and finally along the direction of the maximum principal *in-situ* stress. The fluid pressure and the *in-situ* stress determine the stress distribution near the crack tip and further determine the SIFs. When the crack is inclined to the maximum principal *in-situ* stress, the direction of the maximum circumference stress at the crack tip is also inclined. It makes the crack start to deflect according to the maximum circumferential stress criterion. With the propagation of the fluid-driven crack, the direction of the maximum circumference stress changes gradually under the effects of the *in-situ* stress and the fluid pressure. It is in the direction of the maximum principal *in-situ* stress that the circumferential stress finally gets its maximum value and the deflection process finishes.

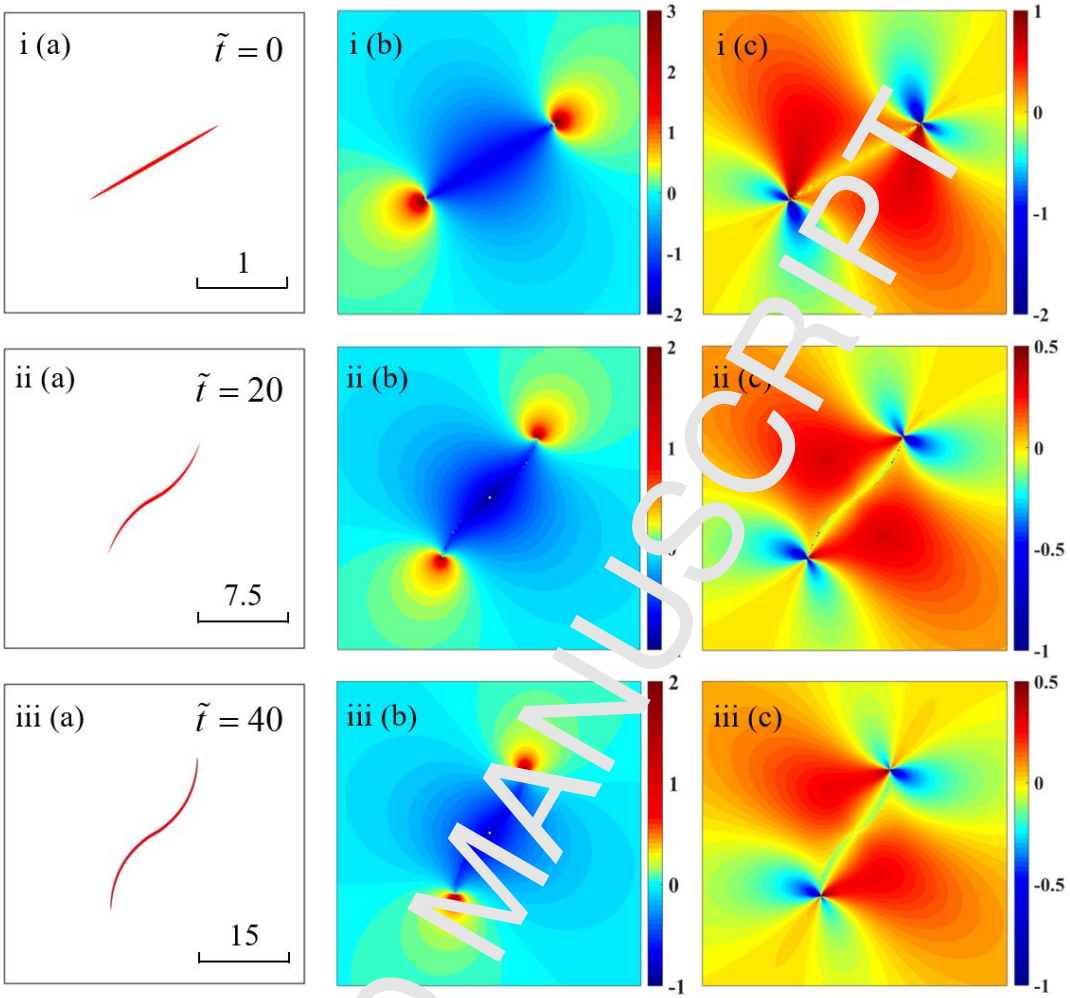

Fig. 4. (a) Crack trajectories, (b) hydrostatic stress field and (c) shear stress field for (is) $\tilde{t}=0$, (ii) $\tilde{t}=20$ and (iii) $\tilde{t}=40$, respectively. The contours indicate the magnitude of the stress.

3.2. Inclination angle

As mentioned in subsection 3.1, the 'deflection region' is a representation of the process in which an inclined crack turns its direction towards the maximum principal stress. To measure the 'deflection region', as shown in Fig. 5(a), dimensionless quantities $\tilde{l}$, $\tilde{l}_1$ and $\tilde{l}_2$ are used, which represent half the curved crack length, half the length of region boundary parallel to the direction of σ_1^∞, and half the length of region boundary parallel to the direction of σ_2^∞, respectively. The cracks with the

inclination angle varying from 25 degrees to 60 degrees are simulated to evaluate the effect of inclination angle on the crack deflection. The parameters used in this simulation are the same as those listed in subsection 3.1. As shown in Fig. 5(b), the deflection region expands dramatically with the increase of the inclination angle. This phenomenon is more apparent when the inclination angle is larger than 45 degrees.

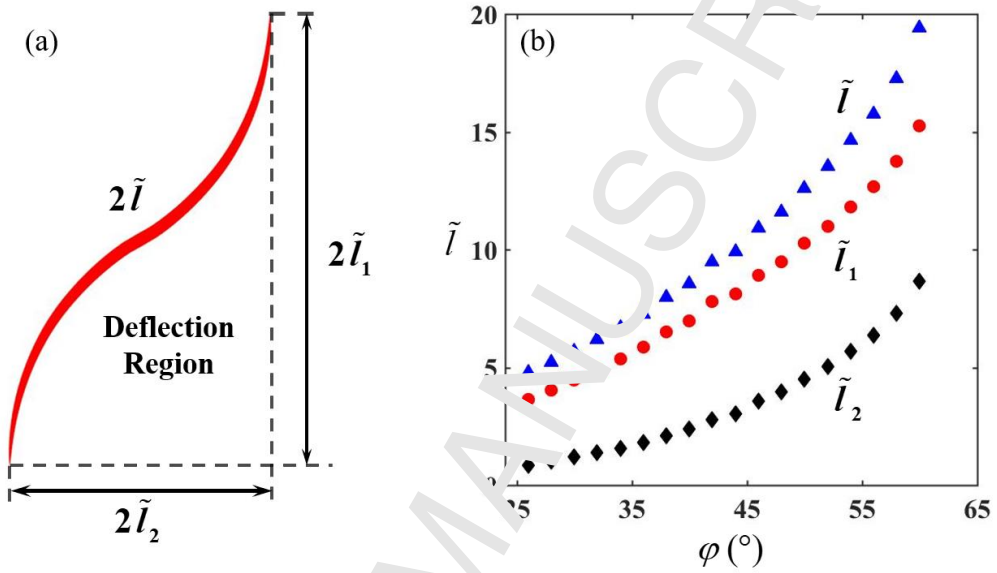

Fig. 5. (a) Schematic of the deflection region. $2\tilde{l}$ is the dimensionless crack length, $2\tilde{l}_1$ is the dimensionless length in the direction of σ_1^∞ and $2\tilde{l}_2$ is the dimensionless length in the direction of σ_2^∞; (b) dimensionless quantities $\tilde{l}$, $\tilde{l}_1$ and $\tilde{l}_2$ with respect to the inclination angle.

3.3. Fluid viscosity and injection rate

In hydraulic fracturing, fluid viscosity and injection rate are controllable in the field treatment. In toughness-dominant regime, by nondimensionalization and normalization, the dimensionless quantity $\tilde{\eta}$ is derived, which represents the combined effect of fluid viscosity and injection rate. It is thus necessary to clarify the effect of dimensionless viscosity on the deflection region. According to the data of laboratory experiments and field observations, the dimensionless viscosity, $\tilde{\eta}$, varies from 0 to 1000 in real

working conditions [28-31]. Thus, we simulated the deflection process with $\tilde{\eta}$ varying from 0 to 1000 and the inclination angle equaling to 30 degrees. The results of the simulation are plotted in Fig. 6. With the increase of the dimensionless quantity $\tilde{\eta}$, the deflection region evidently undergoes changes in three stages. At first, the deflection region increases dramatically and reaches its maximal value when $\tilde{\eta}$ equals to 172, after which the deflection region decreases dramatically and reaches its minimal value when $\tilde{\eta}$ equals to 240, finally it increases gradually and nearly linearly at the third stage. Therefore, the stages are named as significant prevention stage, significant promotion stage and insignificant prevention stage respectively. The results indicate that by controlling the injection rate and selecting the fracturing fluid, one can quantitatively control the deflection of the fluid-driven crack.

As shown in Fig. 6, with the increase of the dimensionless viscosity, the fluid-driven crack becomes more difficult to deflect owing to the increase of the viscous dissipation. In addition, according to Jeffrey [16], oscillation of crack width occurs in the process of crack deflection, which leads to the intensification of viscous dissipation and the deceleration of the crack propagating speed. In our study, the oscillation is most intense at the point where $\tilde{\eta} = 172$, for which reason Fig. 6 behaves non-monotonically and is divided into three regions. In the real working condition, $\tilde{\eta} = 0$ and $\tilde{\eta} = 1000$ correspond to extreme situations, and the inflection points $\tilde{\eta} = 172$ and $\tilde{\eta} = 240$ are more easily to reach. In the significant prevention stage and the significant promotion stage, the inflection points can be achieved by small adjustments of $\tilde{\eta}$.

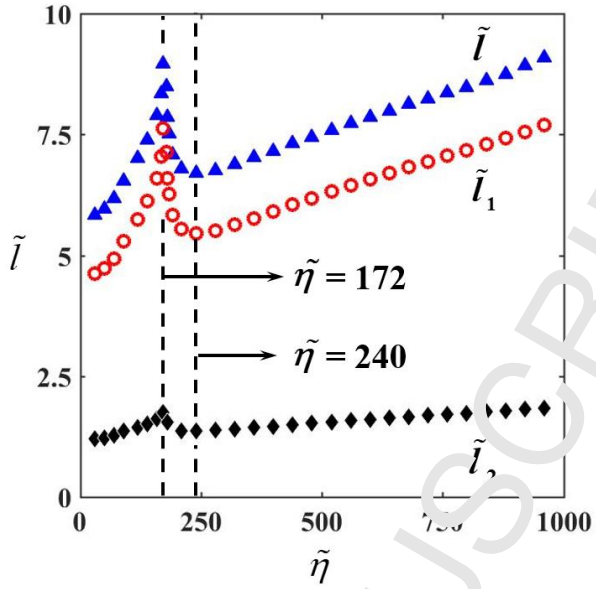

Fig. 6. Dimensionless quantities $\tilde{l}$, $\tilde{l}_1$ and $\tilde{l}_2$ with respect to the dimensionless viscosity $\tilde{\eta}$.

3.4. In-situ stress

The problem is divided into two situations to measure the effect of anisotropic *in-situ* stress on the crack deflection. In the first situation, the stress ratio $\tilde{\sigma}_1^{\infty}/\tilde{\sigma}_2^{\infty}$ remains constant and equals to 10, to measure the effect of *in-situ* stress magnitude on the crack deflection. In the second situation, the maximum principal stress $\tilde{\sigma}_1^{\infty}$ is set to be 0.02, to measure the effect of the stress ratio $\tilde{\sigma}_1^{\infty}/\tilde{\sigma}_2^{\infty}$. During the simulation, the inclination angle equals to 30 degrees and dimensionless viscosity $\tilde{\eta}$ equals to 49. Simulation results are plotted in Fig. 7.

As shown in Fig. 7(a), with the increase of *in-situ* stress, the deflection region decreases dramatically, which means that increase of stress magnitude promotes crack deflection for the instance that under competition with fluid pressure, the increase of the maximum principal stress promotes its effect on the stress distribution near the crack tip, which makes crack propagating direction closer to the direction of the maximum principal stress under maximum circumferential stress criterion. Previous research [32]

explained that for preset parallel cracks with the inclination angle equals to 0, large stress differences prevent deflection caused by interaction among cracks. However, in this study, as shown in Fig. 7(b), with the increase of stress ratio, the deflection region decreases dramatically at the beginning, then becomes almost constant for the ratio being larger than 5. That is to say, for an inclined crack, large stress differences promote crack deflection, which is in contrast with the situation of the for mentioned cracks, and this effect does not become evident when stress ratio is larger than 5.

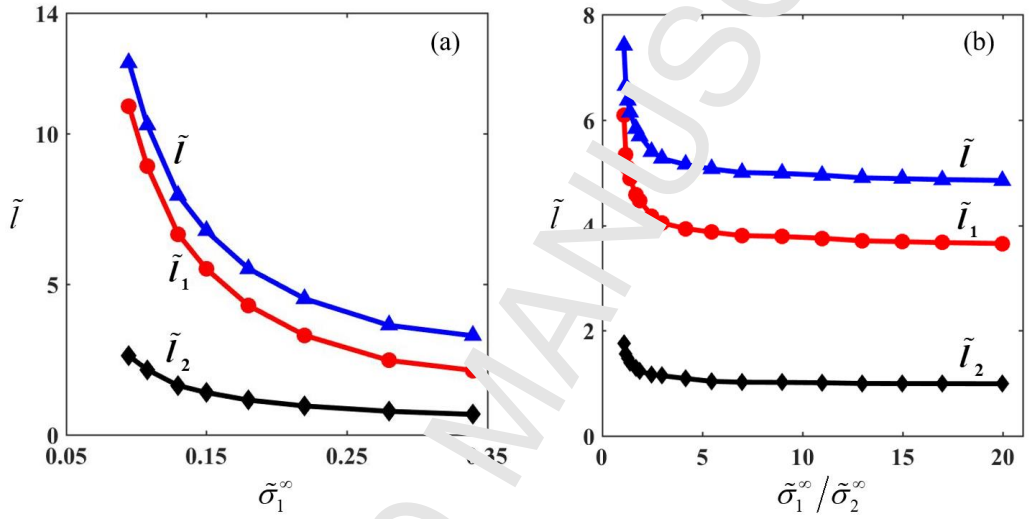

Fig. 7. (a) Dimensionless quantities $\tilde{l}$, $\tilde{l}_1$ and $\tilde{l}_2$ with respect to the magnitude of the maximum principal *in-situ* stress with $\tilde{\sigma}_1^{\infty}/\tilde{\sigma}_2^{\infty}=10$; (b) dimensionless quantities $\tilde{l}$, $\tilde{l}_1$ and $\tilde{l}_2$ with respect to the stress ratio with $\tilde{\sigma}_1^{\infty}=0.2$.

4. Conclusions

The curved trajectory of an inclined fluid-driven crack under anisotropic *in-situ* stress is studied. By using DDM and FDM, the crack deflection is simulated under maximum circumferential stress criterion. The numerical model incorporates the physical effects of fracture, viscosity, injection rate and *in-situ* stress. Results show that an inclined fluid-driven crack curves its trajectory gradually and finally propagates in the direction of the maximum principal stress. A mixed-mode crack of type I and II propagates under the combined effect of fluid pressure and *in-situ* stress. The simulation

also reveals the changes of stress field near the crack during the deflection process. Variable-controlling analysis explains the influences of the factors, respectively. The conclusions are drawn as follows:

(1) The term 'deflection region' is defined to quantify the deflection of a fluid-driven crack.

(2) The inclination angle strongly impacts on the size of the deflection region. Larger inclination angle leads to a larger deflection region, the phenomenon is extremely apparent when the inclination angle is larger than 45 degrees.

(3) The combined effect of injection rate and viscosity of the fracturing fluid is complicated. The process is divided into three stages: significant prevention stage, significant promotion stage and insignificant prevention stage.

(4) Increase of the magnitude and differences of the anisotropic *in-situ* stress can effectively promote the deflection of the inclined fluid-driven crack. And the effect is not significant if the stress ratio is large enough.

(5) The crack propagating direction is dominated by the combined effect of fluid pressure and *in-situ* stress via the stress field near the crack tip. The distribution of stress field caused by fluid pressure is negligible compared with the *in-situ* stress at a distance that nearly equals to the crack length.

This study provides a systematic simulation of the deflection process of an inclined fluid-driven crack. The results clarify the effects of inclination angle, anisotropic *in-situ* stress, fluid viscosity and fluid injection rate on the crack trajectories. It may help in predicting the crack trajectories and in controlling the crack deflection.

Acknowledgement

This work is jointly supported by the National Natural Science Foundation of China (NSFC, Grant No. 11872363, 51861145314), the Chinese Academy of Sciences (CAS) Interdisciplinary Innovation Team Project, the CAS Key Research Program of Frontier Sciences (Grant No. QYZDJ-SSW-JSC019), and the CAS Strategic Priority Research

Program (Grant No. XDB22040401).

Appendix A

Equation (4) is widely used [12,13] in elastic rock-deformation theory to solve the displacement discontinuities. For given boundary conditions of stress, D_i can be solved by Eq. (4), which can be written in component form as follows:

$$T_{jk}(\xi)=\int_S \Xi_{jki}(\xi,\zeta)D_i(\zeta)\mathrm{d}S(\zeta), \tag{A1}$$

where the displacement discontinuity D_i at the point ζ contributes its influence on the stress field T_{jk} at the point ξ through the "displacement-stiffness tensor", Ξ_{jki}. The equation is derived from the solutions of Lord Kelvin's problem [33], that is, the displacement field and the stress field caused by a single force acting in the interior of an infinite solid:

$$U_i = A_{ik} f_k,\ T_{ij} = \vartheta_{ijk} f_k, \tag{A2}$$

in which U_i is the vector of displacement. Due to the existence of crack, the displacement discontinuity can be expressed as $D_i = U_i^- - U_i^+$. f_k is the external force vector. The rank-two tensor A_{ik} and the rank-three tensor ϑ_{ijk} represent the influence of the single force on the displacement field and the stress field, respectively. The solutions in plain-strain [23] are expressed as follows:

$$A_{ik}=\frac{1}{4\pi\mu(\lambda+2\mu)}\left[-\delta_{ik}(\lambda+3\mu)\ln r+(\lambda+\mu)r_{,i}r_{,k}\right], \tag{A3}$$

$$\vartheta_{ijk}=\frac{-1}{2\pi(\lambda+2\mu)r}\left[\mu\left(r_{,j}\delta_{ik}+r_{,i}\delta_{jk}-r_{,k}\delta_{ij}\right)+2(\lambda+\mu)r_{,i}r_{,j}r_{,k}\right], \tag{A4}$$

where λ and μ are the Lamé's constants, δ_{ij}, δ_{ik} and δ_{jk} are the Dirac functions, r is the position coordinate. One can derive Eq. (A1) by eliminating f_k in Eq. (A2) and then integrating along the crack boundary. As shown in Eq. (8), the

displacement discontinuities along the crack is obtained by equating the net pressure of fluid to the normal stress on the crack surfaces in Eq. (7).

References

[1] C.H. Yew, X. Weng, Mechanics of hydraulic fracturing, Gulf Professional Publishing, Oxford, 2014.

[2] S.A. Khristianovic, Y.P. Zheltov, Formation of vertical fractures by means of highly viscous fluids, Proceedings of the 4th World Petroleum Congress, Rome, 1955.

[3] E. Detournay, Mechanics of hydraulic fractures, Annu. Rev. Fluid Mech. 48 (2016) 311-339.

[4] E. Detournay, Propagation regimes of fluid-driven fractures in impermeable rocks, Int. J. Geomech. 4 (2004) 35-45.

[5] V.C. Tsai, J.R. Rice, A model for turbulent hydraulic fracture and application to crack propagation at glacier beds, J. Geophys. Res. 115 (2010) F03007.

[6] D. Garagash, E. Detournay, The tip region of a fluid-driven fracture in an elastic medium, Trans. ASME J. Appl. Mech. 67 (2000) 183-192.

[7] B. Lecampion, E. Detournay, An implicit algorithm for the propagation of a hydraulic fracture with a fluid lag, Comput. Methods Appl. Mech. Engrg. 196 (2007) 4863-4880.

[8] W.H. Shen, F.Q. Yang, Y.Y. Zhao, Unstable crack growth in hydraulic fracturing: The combined effects of pressure and shear stress for a power-law fluid, Eng. Fract. Mech. https://doi.org/10.1016/j.engfracmech. 2018. 11. 032.

[9] W.H. Shen, Y.P. Zhao, Quasi-static crack growth under symmetrical loads in hydraulic fracturing, Trans. ASME J. Appl. Mech. 84 (2017) 081009.

[10] W.H. Shen, Y.P. Zhao, Combined effect of pressure and shear stress on penny-shaped fluid-driven cracks, Trans. ASME J. Appl. Mech. 85 (2018) 031003.

[11] B. Lecampion, J. Desroches, Simultaneous initiation and growth of multiple radial hydraulic fractures from a horizontal wellbore, J. Mech. Phys. Solids 82 (2015) 235-258.

[12] K. Wu, J.E. Olson, Simultaneous multifracture treatments: Fully coupled fluid

flow and fracture mechanics for horizontal wells, SPE J. 20 (2015) 337-346.

[13] K. Wu, J.E. Olson, Mechanisms of simultaneous hydraulic fracture propagation from multiple perforation clusters in horizontal wells, SPE J. 21 (2016) 1000-1008.

[14] A.P. Peirce, A.P. Bunger, Interference fracturing: Nonuniform distributions of perforation clusters that promote simultaneous growth of multiple hydraulic fractures, SPE J. 20 (2015) 384-395.

[15] R.G. Jeffrey, A.P. Bunger, B. Lecampion, et al., Measuring hydraulic fracture growth in naturally fractured rock, SPE Annual Technical Conference and Exhibition, New Orleans, 2009.

[16] R.G. Jeffrey, X. Zhang, M.J. Thiercelin, Hydraulic fracture offsetting in naturally fractures reservoirs: Quantifying a long recognized process, SPE Hydraulic Fracturing Technology Conference, The Woodlands, 2009.

[17] L.N.Y. Wong, H. Einstein, Systematic evaluation of cracking behavior in specimens containing single flaws under uniaxial compression, Int. J. Rock Mech. Min. Sci. 46 (2009) 239-249.

[18] da Silva B. Gonçalves, H. Einstein, Physical processes involved in the laboratory hydraulic fracturing of granite: Visual observations and interpretation, Eng. Fract. Mech. 191 (2018) 125-142.

[19] W.L. Medlin, J. Masse, Laboratory investigation of fracture initiation pressure and orientation, SPE J. 19 (2019) 129-144.

[20] Y. Li, S. Yang, W. Zhao, W. Li, J. Zhang, Experimental of hydraulic fracture propagation using fixed-point multistage fracturing in a vertical well in tight sandstone reservoir, J. Petrol. Sci. Eng. 171 (2018) 704-713.

[21] A. Zang, O. Stephansson, Stress field of the earth's crust, Springer, Berlin, 2010.

[22] G.K. Batchelor, An introduction to fluid dynamics, Cambridge University Press, Cambridge, 2000.

[23] S.L. Crouch, A.M. Starfield, Boundary element methods in solid mechanics,

George Allen & Unwin, London, 1983.

[24] F. Erdogan, G.C. Sih, On the crack extension in plates under plane loading and transverse shear, Trans. ASME J. Basic Eng. 85 (1963) 519-527.

[25] Y.P. Zhao, Modern continuum mechanics, Science Press, Beijing, 2016.

[26] A. Livne, E. Bouchbinder, I. Svetizky, J. Fineberg, The near-tip fields of fast cracks, Science 327 (2010) 1359-1363.

[27] P. Zuo, Y.P. Zhao, A phase field model coupling lithium diffusion and stress evolution with crack propagation and application in lithium ion battery, Phys. Chem. Chem. Phys. 17 (2015) 287-297.

[28] A. Koesoemadinata, G. El-Kaseeh, N. Banik, et al, Seismic reservoir characterization in marcellus shale, SEG Annual Meeting, San Antonio, 2011.

[29] Y. Abousleiman, M. Tran, S. Hoang, et al. Geomechanics field and laboratory characterization of Woodford Shale: The next gas play, SPE Annual Technical Conference and Exhibition, Anaheim, 2007.

[30] B.C. Ames, A.P. Burger, Role of turbulent flow in generating short hydraulic fractures with high net pressure in slickwater treatments, SPE Hydraulic Fracturing Technology Conference, Woodlands, 2015.

[31] W. Li, Z. Jin, G. Cusatis, Size effect analysis for the characterization of Marcellus shale quasi-brittle fracture properties, Rock Mech. Rock Eng. 52(2019) 1-18.

[32] A.P. Bunger, X. Zhang, R.G. Jeffrey, Parameters affecting the interaction among closely spaced hydraulic fractures, SPE J. 17 (2012) 292-306.

[33] L.D. Landau, E.M. Lifshitz, Theory of elasticity, Pergamon Press, Oxford, 1986.

AUTHOR DECLARATION

We wish to confirm that there are no known conflicts of interest associated with this publication and there has been no significant financial support for this work that could have influenced its outcome.

We confirm that the manuscript has been read and approved by all named authors and that there are no other persons who satisfied the criteria for authorship but are not listed. We further confirm that the order of authors listed in the manuscript has been approved by all of us.

We confirm that we have given due consideration to the protection of intellectual property associated with this work and that there are no impediments to publication, including the timing of publication, with respect to intellectual property. In so doing we confirm that we have followed the regulations of our institutions concerning intellectual property.

We understand that the Corresponding Author is the sole contact for the Editorial process (including Editorial Manager and direct communications with the office). He is responsible for communicating with the other authors about progress, submissions of revisions and final approval of proofs. We confirm that we have provided a current, correct email address which is accessible by the Corresponding Author and which has been configured to accept email from yzhao@imech.ac.cn

Signed by all authors as follows:

Jingang Sun, Wenhao Shen, Yapu Zhao

May 16, 2019